AEROELASTIC TAILORING OF AN NLF FORWARD SWEPT WING

DLR contribution to LuFo IV joint research project AeroStruct

T. Wunderlich, DLR Institute of Aerodynamics and Flow Technology, Braunschweig, Germany

S. Dähne, DLR Institute of Composite Structures and Adaptronic, Braunschweig, Germany

Abstract

This article introduces the application of a multidisciplinary analysis (MDA) process chain based on high fidelity simulation methods for the aeroelastic tailoring of an natural laminar flow (NLF) forward swept wing. With this approach the interactions between aerodynamics, loads and structural sizing are considered in the wing analysis. The resulting process enables an integrated aerostructural wing design including aeroelastic tailoring using carbon fiber reinforced plastics (CFRP).

The main feature of the process chain is the hierarchical decomposition of the problem into two levels. On the highest level the orthotropy direction of the composite structure will be analysed. The lower level includes the wing box sizing for essential load cases considering the static aeroelastic deformations. Thereby, the wing box sizing can be performed with a given ply share of the laminate or a ply share optimization. Additionally, the airfoil shapes are transferred from a given NLF wing design. The natural laminar flow is considered by prescribing laminar-turbulent transition locations. The process chain evaluates the wing mass, the lift-to-drag ratio under cruise flight conditions and the corresponding design mission fuel consumption.

Results of aerostructural wing design studies and optimizations are presented for an NLF forward swept wing aircraft configuration. The aerostructural wing optimization with 3 orthotropy angles as design parameters shows a wing mass reduction in the order of 8 % and a design mission fuel consumption reduction in the order of 4 % in comparison to the aeroelastic tailored wing design of the reference aircraft.

1 INTRODUCTION

The environmental impact of aviation increases with the rapid growth of air travel and transport. For this reason efficiency of future air transport must be improved significantly. The research and development of future transport aircraft have to meet this challenge. A Strategic Research Agenda has been developed by the "Advisory Council for Aeronautics Research in Europe" (ACARE). The goals of the European aeronautical research have been formulated in this research agenda and have been published in the "Vision 2020" [1], [2] and the "Flightpath 2050" [3]. In order to protect the environment and the energy supply a 50 % reduction of the CO_2 emissions per passenger kilometer has been requested for the year 2020 based on the values of the year 2000. The airframe contribution should be in the order of 20 % to 25 % in terms of fuel consumption reduction.

To achieve these challenging goals the development timescales for new technologies including new aircraft concepts have to be reduced significantly. For the assessment of an aircraft configuration it is essential to consider all relevant disciplines and their interactions on overall aircraft level. The consideration of new technologies and aircraft concepts requires a physics-based approach because no statistics are available anymore. In order to represent the physics in a realistic manner, accurate simulation tools have to be applied. This inherently leads to increased computational cost. The development of accurate and fast numerical simulation and analysis processes is getting more and more important. In this context new capabilities in the areas of process architecture, program interfaces, parallelization and the usage of high performance computing are required.

The combination of increasing computer resources and advanced numerical simulation tools enables the accurate prediction of flight performance of a transport aircraft configuration [4]. The use of these high fidelity simulation programs for aerodynamic design and optimization has been demonstrated in the MEGADESIGN project (Kroll et al. [5], [6], [7], [8] and Gauger [9]). State of the art high fidelity analysis methods already routinely include fluid-structure coupling of the aircraft wing for a given structural model. The consideration of fluid-structure interactions gets more important for the accurate performance and load prediction of highly flexible wings.

The work on aeroelastic tailoring is summarized by Shirk et al. [10]. In this publication aeroelastic tailoring is described as *"...embodiment of directional stiffness into an aircraft structural design to control aeroelastic deformation, static or dynamic, in such a fashion as to affect the aerodynamic and structural performance of that aircraft in a beneficial way."*. Additionally, the advantages of composite materials on forward swept wings are explained.

Tailoring the primary stiffness direction relative to the structural reference axis introduces a bending-torsion coupling that can be used to counteract the susceptibility of forward swept wings to static divergence. Several approaches are known to tailor the primary stiffness direction. The most common approach is to tailor the whole composite stack. Jutte et al. [11] distinguishes global (uniform) and local (non-uniform) tailoring. Global tailoring approaches are widely used and investigated, but new manufacturing techniques such as automated fiber placement, allows to use different orientations at different positions.

Dähne et al. [12] investigated the influence of global aeroelastic tailored composites on structural mass. In the study an automated structural sizing process has been applied with the simplification that the aerodynamic loads remain fix.

To improve the aerodynamic efficiency of commercial aircraft modern technologies for drag reduction have to be applied. A short overview of aerodynamic wing design and corresponding technologies is given for example by Horstmann and Streit [13]. One of the most promising drag reduction technology is laminar flow control (LFC). The potential of this technology for drag reduction of commercial aircraft has been described by Schrauf [14] and Green [15] for example.

In the DLR project LamAiR [16] the concept of forward sweep for laminar wings as proposed by Redeker and Wichmann [17] shows significant potential for efficiency improvements. In this project a multidisciplinary wing design of a forward swept wing having NLF and a composite structure including aeroelastic tailoring has been performed. The results are published by Kruse et al. [18].

In striving for the capability to assess new wing technologies by development and application of a MDA process chain has been one of the main topics in DLR's contribution to the LuFo IV joint research project AeroStruct. In the scope of the project a process chain for multidisciplinary wing analysis considering new wing technologies such as forward sweep, NLF, composite materials and aeroelastic tailoring has been developed. In the setup of the process chain it was made sure that the aerodynamic loads entering the structural sizing always result from fluid-structure coupled simulations. Wunderlich [19] showed that this has crucial influence on the multidisciplinary wing optimization results.

2 PROCESS CHAIN FOR AEROSTRUCTURAL WING ANALYSIS

An integrated process chain for aerostructural wing analysis based on high fidelity simulation methods has been used. This process chain has been published by Wunderlich et al. [20] and is presented here again with the focus on aeroelastic tailoring. The integrated process chain can be characterized by the following items:

- Usage of a central file format for parametric aircraft description,
- Automated grid generation for aerodynamic simulation,
- Automated structural model generation for structural simulation,
- Parallel static aeroelastic analysis for an arbitrary number of load cases,
- Structural wing box sizing for composite structures,
- Aeroelastic tailoring by orthotropy angle variation,
- Consideration of NLF by prescribing laminar-turbulent transition locations.

In Fig. 1 the process chain is illustrated with an XDSM-diagram (Extended Design Structure Matrix) [21]. This type of diagram combines the information of process flow between computational components with the information of data dependency. Each component in the diagram takes input data from the vertical direction and provides output data from the horizontal direction. Input and output data are marked by parallelograms. Thick gray lines show the data flow. Thin black arrows indicate the process flow, and a numbering system is used to define the order in which the components are executed.

The starting point for an aerostructural wing analysis is normally a detailed geometrical model of a given reference aircraft configuration. From this non-parametric model a fully parametric description of the aircraft using the Common Parametric Aircraft Configuration Schema (CPACS) has to be generated manually or with a program in an automated way. Furthermore, the initial vector of design parameters $\vec{x}^{ini}$ is determined by the reference aircraft configuration. The load case definitions for the structural sizing have to be identified and stored in the CPACS dataset.

All disciplinary simulation programs in the process chain provide interfaces to this central hierarchical ASCII text file format. In Sect. 2.2 the parametric model and the CPACS dataset are described in more detail.

The driver component controls the optimization iteration and is represented in Fig. 1 by the blue box. Based upon a design parameter variation and a following transfer to the CPACS dataset, the disciplinary models are built or updated automatically. Thereby, the vector of design parameters $\vec{x}$ describes the wing planform including twist and airfoil thickness distributions and the orthotropy angles of the composite structure. In this article the wing planform is held constant and the aeroelastic tailoring is investigated by orthotropy angle studies.

The static aeroelastic analysis is then run in parallel for all load cases including the design point under cruise flight conditions. In the actual implementation, the process chain is limited to steady state maneuver load cases and only the wing-fuselage configuration is analysed within the high-fidelity simulation process.

For each load case the surface pressure distribution and aerodynamic coefficients of the wing are determined

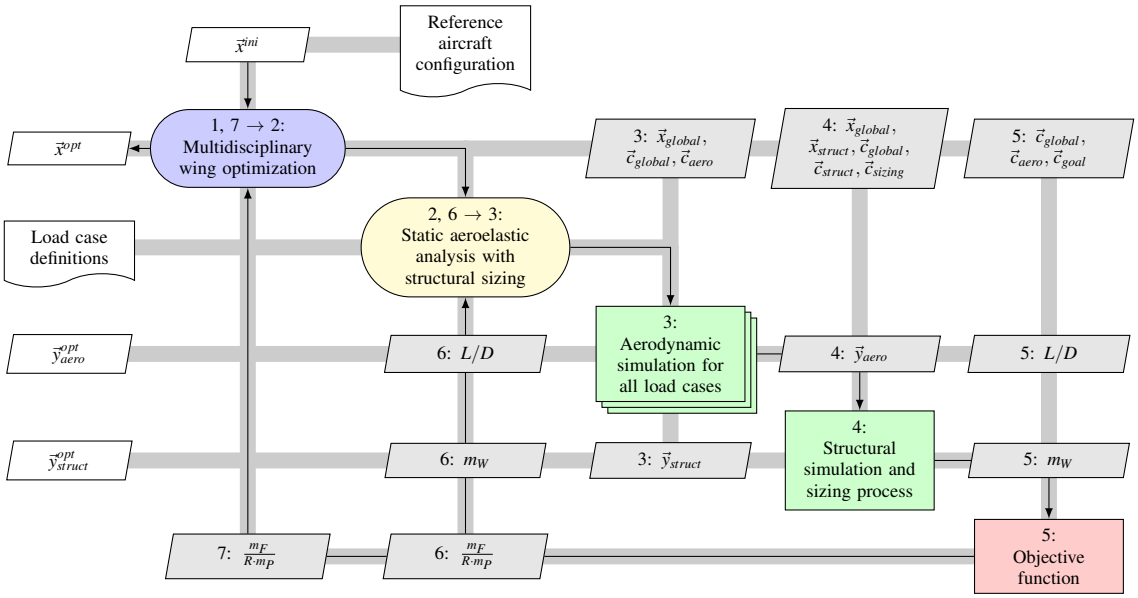

Fig. 1: Flow chart of the process chain for aerostructural wing analysis.

by solving the Reynolds-averaged Navier–Stokes equations (RANS) within a numerical flow simulation. Elastic characteristics of the wing and its internal loads are determined using the finite element method (FEM). Subsequently, the wing mass is deduced by processing these internal loads. The interactions between the aerodynamic forces and the structural deformations of the elastic wing are taken into account in the static aeroelastic analysis. The fluid-structure interaction belongs to the category of loosely coupled analysis as described in [22] and [23]. Thereby, the fluid-structure coupling loop stops when the values for the lift-to-drag ratio, wing mass and fuel consumption are converged. The fluid-structure coupling loop is shown in Fig. 1 by the yellow box.

The main results of the parallel static aeroelastic analysis are the wing mass m_W and the deformed wing shape for the design point under cruise flight conditions, which is normally called "1g-flight shape". Based on this 1g-flight shape the aerodynamic performance in terms of lift-to-drag ratio L/D is determined.

The last step in the process chain is the evaluation of the objective function f for the multidisciplinary assessment of the wing design.

2.1 Flight Mission

For the evaluation of the objective function a simplified model of the flight mission has been used. This model is described in the textbook by Raymer [24] and is often used for preliminary aircraft design.

In this work, the flight mission consist of five segments. Table 1 gives an overview of these flight mission segments and the corresponding aircraft mass fractions. With the exception of the cruise flight segment the values for the aircraft mass fractions have to be prescribed depending on the aircraft and mission.

Segment number	Mission segment	Aircraft mass fraction
1	Warm-up, taxi and take-off	m_1/m_0
2	Climb and accelerate	m_2/m_1
3	Cruise	m_3/m_2
4	Descent for landing	m_4/m_3
5	Landing and taxi	m_5/m_4

Table 1: Flight mission segments and mass fractions.

For the cruise flight segment a constant flight speed V and a given constant lift coefficient C_L have been assumed. The flight speed V is determined by the selected design cruise Mach number Ma and the flight altitude H at the beginning of cruise flight. In combination with the assumption of constant thrust specific fuel consumption $TSFC$ this leads to the well known Breguet range equation:

$$(1) \quad R = \frac{1}{g} \frac{V}{TSFC} \frac{L}{D} \ln \frac{m_2}{m_3}$$

The lift-to-drag ratio L/D of the aircraft for the given lift coefficient C_L and the wing mass m_W are results of the parallel static aeroelastic analysis. Furthermore, the selected flight mission corresponds to the design mission. The outcome of this is that the aircraft mass m_0 at the start of the mission is equivalent to the maximum take-off mass m_{MTO}. For an aircraft the maximum take-off mass m_{MTO} is the sum of the residual mass m_{Res} (structural mass without the wing), the wing mass m_W, the payload m_P, the fuel mass m_F

and the reserve fuel mass $m_{F,res}$:

$$(2) \quad m_{MTO} = m_{Res} + m_W + m_P + m_F + m_{F,res}$$

In the presented applications the maximum take-off mass m_{MTO} is held constant. Furthermore, the residual mass ratio m_{Res}/m_{MTO} is also assumed to be constant, because the analysis is limited to the wing. In accordance with the simple model of the flight mission, the reserve fuel mass fraction $m_{F,res}/m_F$ is assumed to be constant as well. The fuel mass m_F corresponds to the fuel mass which is required for the design mission and has been calculated with the following equation:

$$(3) \quad m_F = m_0 - m_5 = m_{MTO} - m_5$$

For the transfer of the simulation results to the aircraft level the three following assumptions have been made.

Firstly, it has been assumed that the tailplane lift coefficient $C_{L,T}$ is constant. This means that the adaptation of tailplane lift for aircraft trimming has been neglected. The sum of wing and fuselage lift coefficients $C_{L,W} + C_{L,F}$ results from the flow simulation and matches the prescribed target lift coefficient for the cruise flight.

Secondly, a constant sum of tailplane and engine cowling drag coefficients (here denoted by $C_{D,res}$) has been assumed. The sum of wing and fuselage drag coefficients $C_{D,W} + C_{D,F}$ is a result of the flow simulation and includes pressure and viscous parts. With these assumptions the aerodynamic performance in terms of lift-to-drag L/D ratio is calculated with the following equation:

$$(4) \quad \frac{L}{D} = \frac{C_L}{C_D} = \frac{\overbrace{C_{L,W} + C_{L,F}}^{\text{flow simulation}} + \overbrace{C_{L,T}}^{=const.}}{\underbrace{C_{D,W} + C_{D,F}}_{\text{flow simulation}} + \underbrace{C_{D,T} + C_{D,E}}_{C_{D,res}=const.}}$$

Thirdly, the wing mass m_W is the sum of the wing box mass $m_{W,box}$ and the secondary wing masses $m_{W,sec}$. The secondary wing mass consists of the wing leading and trailing edge masses, which have been prescribed in terms of mass per projected area. Additionally, the wing box mass is computed based on the sized finite element (FE) model and is multiplied by a correction factor of 1.25 to get a more realistic wing mass. This correction factor accounts for additional structural mass, which is not modeled in the idealized wing box model.

2.2 Parametric Model

For the parameterization of the aircraft the Common Parametric Aircraft Configuration Schema (CPACS) [25] has been selected. This aircraft parameterization scheme uses the widely spread Extensible Markup Language (XML). Hence, the CPACS dataset represents a hierarchical organized ASCII text file format.

The usage of CPACS offers a generic and fully parametric description of the aircraft. The geometrical description in CPACS is section based and guide curve geometries can additionally used for the surface lofting. The resulting quality of the outer surface geometry is appropriate for aerodynamic simulations with CFD methods.

In CPACS the inner geometry is defined based on the outer geometry description. This includes for example the parametric arrangement of spars and ribs. Parameters to specify the orientation of orthotropic materials are part of the CPACS description. Also the used materials with their properties have to be defined in the CPACS dataset. The structural model generation process is linked to the CPACS dataset and is introduced in Sect. 2.4.

For the aerodynamic simulations a CAD model has been built automatically within the commercial software system CATIA® V5 based on the geometry description in CPACS. This parametric CAD model represents an equivalent representation of the geometrical description in CPACS with the same parametric description. The main task of the CAD model is the computation of the resulting surfaces and intersections for a given set of geometrical parameters in CPACS. In addition the CAD model includes the auxiliary geometry for the aerodynamic grid generation process.

2.3 Aerodynamic Simulation

The transonic flow around the wing-fuselage configuration is simulated with the DLR TAU-Code [26], [27], [28], which has been developed at the DLR Institute of Aerodynamics and Flow Technology. The TAU-Code solves the compressible, three-dimensional Reynolds-averaged Navier–Stokes equations. It is a well established tool for aerodynamic applications at DLR, universities and European aerospace industry [29], [30], [4]. The TAU-Code uses a vertex centered dual mesh formulation. This formulation supports tetrahedral, prismatic, pyramidal and hexahedral elements. For spatial approximation, a finite volume method with second order upwind or central discretization is used. The turbulence models implemented within the TAU-Code include one- and two-equation eddy-viscosity models and Reynolds-stress models (RSM).

For the flow simulation within the aerostructural process chain the central discretization schema and the negative Spalart–Allmaras turbulence model [31] is currently being used.

In Fig. 2 the surface grid of the reference aircraft configuration is shown as an example. It also includes some details of the leading and trailing edge.

To minimize the number of grid points an O-O-topology is used. Each airfoil section is discretized with 170 points. The resulting aerodynamic grid consists of $2.5 \cdot 10^6$ points. This grid resolution represents an appropriate trade-off between accuracy and computing effort for wing design studies.

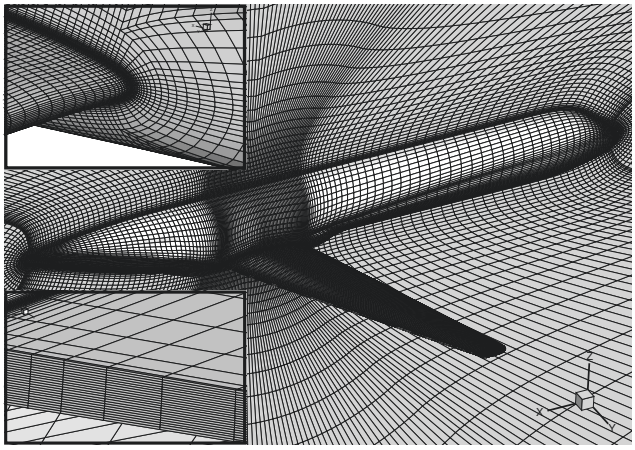

Fig. 2: Aerodynamic surface grid of the reference aircraft configuration with some details of the leading and trailing edge.

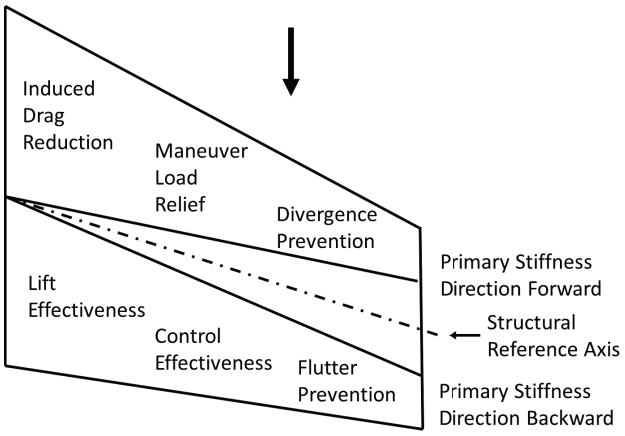

Fig. 3: Effects of aeroelastic tailoring adopted from Shirk et al. [10].

2.4 Structural Model Generation Process

For the generation of structure models, the software DELiS (Design Environment for thin-walled Lightweight Structures) has been selected. The core of DELiS is a parametric model generator that supports various levels of detail. Based on a CPACS dataset, DELiS creates an abstract and object oriented model of the aircraft. This model contains all the structurally relevant CPACS information and enriches it with required data for finite elements. Due to the abstract and FE-centric definition of the lightweight structure, models for various FE solvers can be created, such as MSC Nastran™ and ANSYS® [32].

The approach for introducing a bending-torsion coupling is to rotate the primary stiffness direction of the material. Thereby the complete composite layup is rotated around the z-axis. This rotation leads to a structural coupling of wing bending and torsion. The rotation is realized by defining a reference coordinate system for the material orientation in the finite element model. The material properties are defined symmetrical and balanced with respect to the reference coordinate system. The global structural bending-torsion coupling of the wing is then obtained by rotating the whole reference system around its z-axis.

Fig. 3 shows the effects of aeroelastic tailoring by rotating the primary stiffness direction.

2.5 Structural Analysis and Sizing

The aim of the structural sizing and optimization process is the minimization of the wing box mass $m_{W,box}$ with respect to a set of failure criteria. External loads are calculated within the flow simulation and afterwards mapped onto the automatic generated FE model. Internal loads are calculated with linear-static FE calculations. Subsequently the FE model with its geometry, material properties and loads is passed to the sizing and optimization module.

The module for sizing and optimization is based on fast analytic evaluations at panel component level. Therefore, an analytical representation of stringer stiffened panels is used to evaluate failure criteria for each optimization component. It should be noticed that skin and stringer are optimized together. With this approach a change in the stiffness distribution between skin and stringer results in stress redistribution so an optimum design can be found. Structure mechanical criteria for global buckling, local buckling and maximum strain for skin and stiffener are used for the sizing of the structural components.

Fast analytical evaluations allow a brute force method to find the lightest panel configuration. The structural design parameters are therefore discretized between their actual bounds. For each optimization region a list of all possible design concepts is created and sort by structural mass. For each concept the failure criteria are evaluated, beginning at the lightest design. The first design fulfilling all criteria is the lightest concept for the present load.

Damage tolerance constraints are covered by adapted strain allowable. For the strain allowable at ultimate load a conservative value of $3500\,\mu m/m$ has been chosen as proposed in Military Handbook [33]. Furthermore, criteria from manufacturing and operations like minimum and maximum height for stringer webs and a minimum skin thickness for repair are considered.

Composite materials are difficult to handle in optimization due to their discrete nature. To handle composite materials in a continuous process a smeared approach is used. The membrane stiffness is based on the ply share. The ply share represents the percentage share of $0°$, $90°$, $+45°$ and $-45°$ plies. Assuming an equal distribution of each ply through thickness leads to the corresponding bending-stiffness based on the membrane stiffness and the thickness.

The ply share can either remain unchanged to ensure a desired material behavior or can be optimized in terms of minimum mass. Thereby, the ply share optimization varies the ply share values and adds an additional structural design variable. This additional degree of freedom can improve the structural design in terms of mass. Minimum

and maximum ply shares in $0°/90°/+45°/-45°$ direction are considered to ensure the validity of common design guidelines like the ten-percent rule [34].

2.6 Fluid-Structure Coupling

The fluid-structure interaction loop to be carried out in each of the parallel static aeroelastic analyses (see Fig. 1) involves the following operations:

1. Compute the aerodynamic loads on the given CFD grid for every load case,
2. Interpolate the loads from the CFD surface grid to the structural model,
3. Perform the structural sizing (once the loads of all load cases are available),
4. Compute the structural deformations for the newly sized structure for every load case and
5. Adjust the CFD volume grid according to the resulting structural deformations.

Then the loop starts over again. In step 2, an efficient classical nearest-neighbor interpolation is applied. It ensures equilibrium of forces on fluid and structural side. The existing defect in the equilibrium of moments is negligible. In step 5, a fast and robust grid deformation method is used which is based on the scattered data interpolation technology using radial basis functions. Based on the occurring structural deformations, a volume spline is determined which is then evaluated in parallel at all CFD volume grid points. Refer to the publication by Barnewitz [35] for more detailed information on the grid deformation method.

For the convergence of the fluid-structure coupling loop several convergence criteria have been used in parallel. A list of all considered physical quantities and their corresponding convergence criteria is shown in Table 2. Once all convergence criteria are fulfilled, the aeroelastic equilibrium is considered to be achieved and the fluid-structure coupling loop is terminated.

Physical quantity		Convergence criterion[a]
Lift-to-drag ratio	L/D	$\frac{\Delta(L/D)}{L/D} \leq 0.001$
Wing mass	m_W	$\frac{\Delta m_W}{m_W} \leq 0.005$
Fuel consumption	FC	$\frac{\Delta FC}{FC} \leq 0.002$

[a] The Δ symbol indicates the difference between the values of two consecutive fluid-structure coupling iterations.

Table 2: Convergence criteria of the fluid-structure coupling.

The selected values represent an appropriate trade-off between accuracy and computing time for the static aeroelastic analyses. The application of the process chain shows 4 to 8 fluid-structure coupling iterations in practice to reach convergence.

3 REFERENCE AIRCRAFT CONFIGURATION

Within the scope of the DLR project LamAiR [16] an aerostructural wing design of an NLF forward swept wing for short and medium range transport aircraft was performed [18]. It was shown, that the forward swept wing design enables for wide extend of laminar flow at transonic flight conditions. By aeroelastic tailoring of the composite wing structure, a divergence free design was achieved.

For the present study of aerostructural wing design, the LamAiR aircraft configuration has been selected as the reference. Furthermore, the top level aircraft requirements and the design mission are identical to this aircraft configuration. Table 3 gives an overview on the top level aircraft requirements.

Design cruise Mach number	$Ma = 0.78$
Design mission payload	$m_P = 150\,\text{PAX}$
Design range	$R = 4815\,\text{km}$
Maximum payload	$m_{P,max} = 150\,\text{PAX} + 5\,\text{t}$
Range with maximum payload	$R_{mP} = 3056\,\text{km}$
Take-off field length	$s_{TOFL} \approx 1900\,\text{m}$
Landing field length	$s_{LFL} \approx 1600\,\text{m}$
Propulsion	CFM56 class turbofan
Airport conformity	FAA Group III and ICAO Code C

Table 3: Top level aircraft requirements of the reference aircraft configuration.

The reference aircraft configuration has a low wing, rear mounted engines and a T-tail as shown in Fig. 4. To fulfill the surface requirements for laminar flow and the requirements for take-off and landing performance, the reference aircraft features a smart leading edge high-lift system as proposed by the DLR Institute of Composite Structures and Adaptive Systems [36].

The selected reference aircraft configuration represents a short and medium range commercial aircraft in the Airbus A320 and Boeing 737 class.

Key figures of the aircraft's flight envelope are summarized in Table 4. Flight envelope data give the basis for the selection of critical load cases for the structural sizing of the wing box.

Altitude		
Max. flight altitude	H_{max}	12500 m
Design speeds		
Max. operating Mach number	Ma_{MO}	0.8
Max. operating limit speed	$V_{MO,CAS}$	350 kn
Design diving Mach number	Ma_D	0.87
Design diving speed	$V_{D,CAS}$	395 kn

Table 4: Key figures of the flight envelope.

The aerodynamic wing design of the reference aircraft

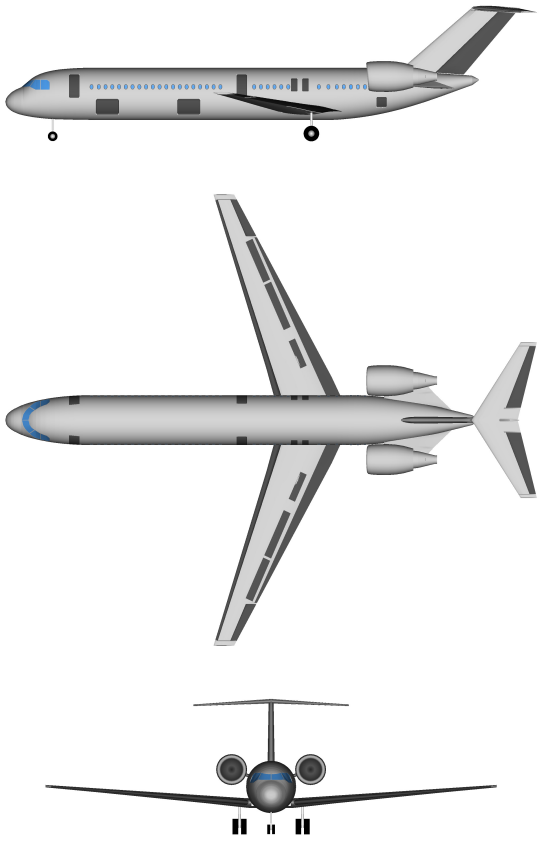

Fig. 4: Reference aircraft configuration.

configuration was published by Kruse et al. [18]. With the objective of drag reduction by maximizing the extension of laminar flow for a design cruise Mach number of $Ma = 0.78$, the choice for a forward swept wing configuration is well-founded. For tapered wings, the forward swept wing design allows the favorably low leading edge sweep angle of $\varphi_{LE} = -17\,^\circ$ for a passive control of cross flow instabilities in the leading edge region. Simultaneously, a sufficiently high sweep angle near the mid-chord shock position in the order of $\varphi = -25\,^\circ$ is maintained, to meet the requirement of low wave drag in cruise flight for realistic wing thickness distributions and lift coefficients. Regarding these aspects, the forward swept wing design offers a clear advantage for NLF design under transonic cruise flight conditions in comparison to backward swept configurations.

The wing box structure of the reference aircraft configuration has been derived from the structural design and sizing of the LamAiR configuration [18]. For the composite wing box the material properties of the CYCOM® 977-2 Epoxy Resin System from Cytec Industries Inc. have been used. The percentage ply share of the composite material is shown in Table 5 for the wing box of the reference aircraft configuration.

The final layout of the structural wing design for the LamAiR configuration came up with a main fiber direction of $-11\,^\circ$ relative to the mean line of the wing box [18]. For the reference aircraft configuration a slightly different value of $\varphi_{OD} \approx -10\,^\circ$ has been selected for the global orthotropy angle of the composite material.

	Dimensionless span coordinate $\eta = 2y/b$	Percentage ply share $0\,^\circ/\pm 45\,^\circ/90\,^\circ$
Upper skin	0.0000 – 0.3876	70/20/10
	0.3876 – 0.8157	60/20/20
	0.8157 – 0.8871	50/30/20
	0.8871 – 0.9584	40/40/20
Lower skin	0.0000 – 0.3520	70/20/10
	0.3520 – 0.7444	60/20/20
	0.7444 – 0.7801	50/30/20
	0.7801 – 0.9584	40/40/20
Front spar	0.0000 – 0.6730	50/30/20
	0.6730 – 0.9584	40/30/30
Rear spar	0.0000 – 0.9584	70/20/10
Ribs	0.0000 – 0.2101	10/80/10
	0.2101 – 0.3163	20/60/20
	0.3163 – 0.3876	30/50/20
	0.3876 – 0.4947	40/40/20
	0.4947 – 0.9584	60/20/20

Table 5: Percentage ply share of the wing box composite material.

4 RESULTS

The introduced process chain, as described in section 2, has been used for aerostructural wing design studies and a orthotropy angle optimization of a forward swept wing aircraft configuration. Thereby, the laminar airfoils from the reference aircraft configuration have been used. To consider the drag reduction of laminar flow the laminar-turbulent transition has been prescribed at a fixed percentage in chord direction. This relative position in chord direction of the laminar-turbulent transition has been held constant during all aerodynamic simulations under cruise flight conditions. The goal of these wing design studies is to investigate the influence of aeroelastic tailoring to the lift distribution, wing deformations, wing mass and design mission fuel consumption.

4.1 Design Task

4.1.1 Design parameters and constraints

The selected design parameters for the aerostructural wing design studies and optimization are:

- Inboard orthotropy angle $\varphi_{OD,inboard}$,
- Middle wing orthotropy angle $\varphi_{OD,middle}$,
- Outboard orthotropy angle $\varphi_{OD,outboard}$.

For the aeroelastic tailoring of the wing the complete orthotropic material including the stringers of the upper and lower wing box skin is rotated. The orthotropy angle of the composite material φ_{OD} is defined relative to the mean line of the wing box at 37.5 % chord. In Fig. 5 the selected definition of design parameters is shown. The aeroelastic tailoring has been applied to the inboard, middle and outboard wing regions. This is achieved by using the orthotropy angles of the composite material $\varphi_{OD,inboard}$, $\varphi_{OD,middle}$ and $\varphi_{OD,outboard}$ to control the bending-torsion coupling of the wing. Thereby, the middle wing region starts at approximately 40 % wing span and ends at approximately 70 % wing span. Consequently the inboard wing region ends at approximately 40 % wing span and the outboard wing region starts at approximately 70 % wing span. In the unswept center wing the orthotropy angle of the composite material remains unchanged at $\varphi_{OD,center} = 0°$.

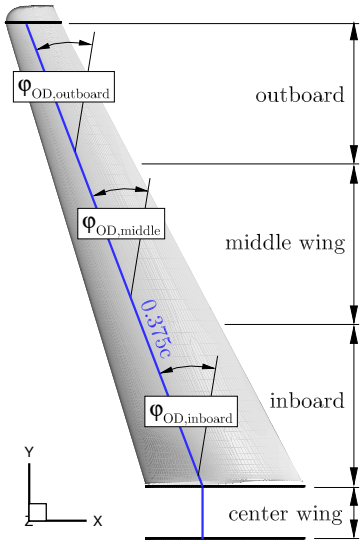

Fig. 5: Definition of design parameters.

The wing design studies and optimization constraints are listed in Table 6. These are based on the top level aircraft requirements of Table 3 and the results of the conceptual aircraft design published in [18]. This includes the specifications of the maximum take-off mass m_{MTO}, wing loading m_{MTO}/S and the cruise Mach number Ma.

For the structural sizing of the wing box three maneuver load cases with minimum and maximum load factors from the certification specifications CS-25/FAR 25 have been selected. The definitions of the cruise flight design point and the selected load cases are specified in Table 7 and are based on the flight envelope of the reference aircraft configuration.

The NLF wing sections have been adopted from the reference aircraft configuration. For the flow simulations, spanwise transition locations are prescribed at $x_T/c = 0.3$ for the inboard wing and $x_T/c = 0.4$ for the middle and outboard wing.

Aircraft		
Maximum take-off mass	m_{MTO}	73 365 kg
Maximum payload	$m_{P,max}$	19 250 kg
Wing loading	m_{MTO}/S	556 kg/m^2
Residual mass ratio	m_{Res}/m_{MTO}	0.4604
Drag coefficient of tailplane and engine cowling	$C_{D,res}$	0.0025
Specific mass of leading edge high lift device	m_{le}/S_{le}	30 kg/m^2
Specific mass of trailing edge high lift device	m_{te}/S_{te}	50 kg/m^2
Relative front spar position	x_{FS}/c	0.15
Relative rear spar position	x_{RS}/c	0.60
Number of ribs	N_{Ribs}	$2 \cdot 27 + 1 = 57$
Design mission		
Mach number	Ma	0.78
Range	R	4815 km
Range cruise segment	R_{23}	3726 km
Lift coefficient aircraft	C_L	0.5
Lift coefficient tailplane	$C_{L,T}$	−0.0022
Thrust specific fuel consumption	$TSFC$	0.0589 kg/(Nh)
Take-off and climb mass fraction	m_2/m_0	0.9589
Descent and landing mass fraction	m_5/m_3	0.9906
Reserve fuel mass fraction	$m_{F,res}/m_F$	0.4604

Table 6: Constraints of the wing design studies and optimization.

The topology of the wing box structure (relative spar positions and number of ribs) and the ply share of the composite material are transferred from the reference aircraft configuration. The values for this percentage ply share of the composite material are presented in Table 5. Within the structural sizing process the wing box topology is held constant. For the structural sizing with fixed ply share, the percentage of ply share is identical to the reference aircraft configuration. Additionally, a structural sizing process including ply share optimization has been applied in the aerostructural process chain. The wing box mass $m_{W,box}$ resulting from the structural sizing process is multiplied by a factor of 1.25 to account for additional masses which are not modeled in the idealized finite element model [37]. This is required to obtain a realistic wing mass for the evaluation of the objective function.

4.1.2 Objective Function

Based on the simplified model for the flight mission as introduced in Sect. 2.1 the fuel consumption FC has been selected as the figure of merit for the aerostructural wing design studies and optimization. The fuel consumption FC is defined here in terms of fuel burn per range and payload $m_F/(R\,m_P)$ for a given range R.

The minimization of the fuel burn is an appropriate objective for the aerostructural wing optimization of future commercial aircraft as shown in [38].

For the calculation of the fuel consumption the required equations are listed in Table 8. Thereby, the fuel mass m_F

Load case	Altitude H	Mach number Ma	Lift coefficient $C_{L,W}+C_{L,F}$	Aircraft mass m	Load factor n
Cruise[a]	10668 m	0.780	0.502	68640 kg	1.0
LC2	0 m	0.717[b]	0.374	73365 kg	2.5
LC3	4725 m	0.772	0.571	73365 kg	2.5
LC4	0 m	0.717[b]	−0.149	73365 kg	−1.0

[a] Design point with laminar-turbulent transition prescription
[b] $V = 1.2 \cdot V_D$ for divergence prevention from CS-25/FAR 25

Table 7: Cruise flight design point and load cases for the structural sizing of the wing.

is computed from the given cruise segment range R_{23} and the lift-to-drag ratio L/D. The payload m_P results from this fuel mass m_F and the wing mass m_W. As mentioned before, the lift-to-drag ratio L/D and the wing mass m_W are outputs of the parallel static aeroelastic analysis. With all these calculated values the fuel consumption per range and payload $m_F/(R\,m_P)$ follows directly from the last equation of Table 8.

Mass fraction cruise	$\frac{m_3}{m_2} = e^{-\frac{g\,TSFC\,R_{23}}{V\,(L/D)}}$
Mass fraction fuel	$\frac{m_F}{m_{MTO}} = 1 - \frac{m_3}{m_2}\,\frac{m_1}{m_{MTO}}\,\frac{m_2}{m_1}\,\frac{m_4}{m_3}\,\frac{m_5}{m_4}$
Mass fraction payload	$\frac{m_P}{m_{MTO}} = 1 - \frac{m_{Res}}{m_{MTO}} - \frac{m_W}{m_{MTO}} - \left(1 + \frac{m_{F,res}}{m_F}\right)\frac{m_F}{m_{MTO}}$
Specific fuel consumption	$FC = \frac{1}{R}\,\frac{m_F}{m_{MTO}}\,\frac{m_{MTO}}{m_P}$

Table 8: Equations for the calculation of fuel consumption.

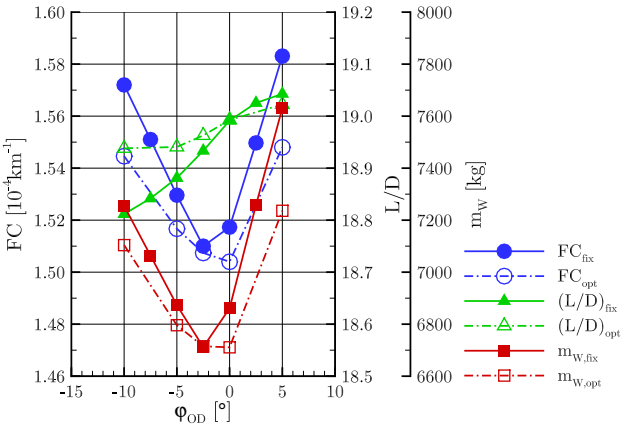

Fig. 6: Fuel consumption, lift-to-drag ratio and wing mass for global orthotropy angle variation with fixed ply share and ply share optimization.

4.2 Global orthotropy angle variation

In this section the results of aeroelastic tailoring by global orthotropy angle variation are presented. The investigations have been performed with the same value for the inboard, middle wing and outboard orthotropy angle. This global orthotropy angle is referred to as orthotropy angle φ_{OD}.

In Fig. 6 the results of fuel consumption, lift-to-drag ratio and wing mass for global orthotropy angle variation with fixed ply share (*solid* line and symbols with index *fix*) and ply share optimization (*dot-dashed* line and symbols with index *opt*) are shown.

The curve of the design mission fuel consumption FC follows the trend of the wing mass m_W curve. This can be explained by the higher sensitivity of the wing mass with subject to the orthotropy angle variation in comparison to the lift-to-drag ratio. The lift-to-drag ratio L/D under cruise flight conditions increases continuously with increasing orthotropy angle due to lift distribution changes in spanwise direction. For the global orthotropy angle variation with fixed ply share the minimum wing mass and fuel fuel consumption is reached for values between $\varphi_{OD} = -5°$ and $\varphi_{OD} = 0°$. The results of he global orthotropy angle variation with ply share optimization show lower values of wing mass and fuel consumption in comparison to the results with fixed ply share. Additionally, the minimum of wing mass and fuel consumption is shifted to values near a global orthotropy angle of $\varphi_{OD} = 0°$.

The influence of the global orthotropy angle variation to the lift distribution has been analysed in terms of the dimensionless spanwise coordinate of the center of lift η_{COL}. In Fig. 7 and Fig. 8 the lift-to-drag ratio and the center of lift under cruise flight conditions are shown for global orthotropy angle variation. Fig. 7 presents the results with fixed ply share and Fig. 8 shows the results with ply share optimization. In both figures the spanwise position of the center of lift for the "jig-shape" (index *jig*) and the elliptical lift distribution (index *ell*) are additionally included. The elliptical lift distribution is the optimum for planar wings in terms of induced drag.

With increasing global orthotropy angle φ_{OD} the center of lift η_{COL} is shifted outboard for the fixed ply share as shown in Fig. 7. The bending-torsion coupling of the forward swept wing without aeroelastic tailoring ($\varphi_{OD} = 0°$) shows an increasing twist angle at the wing tip with increasing wing bending. Hence, the lift distribution and the corresponding center of lift is shifted outboard. Increasing values of the global orthotropy angle φ_{OD} increases this effect. Decreasing values of the global orthotropy angle φ_{OD} lead to decreased bending-torsion coupling and to an in-

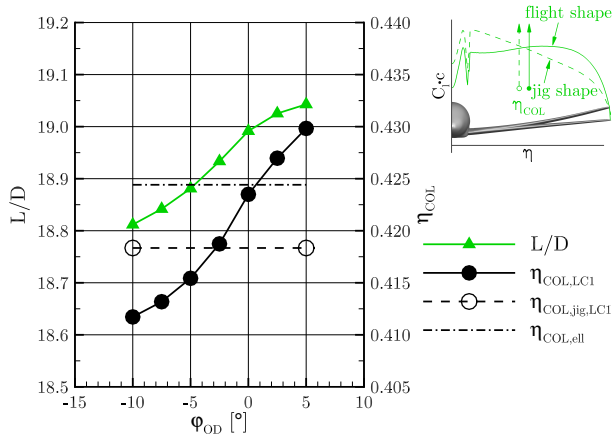

Fig. 7: Lift-to-drag ratio and center of lift under cruise flight conditions for global orthotropy angle variation with fixed ply share.

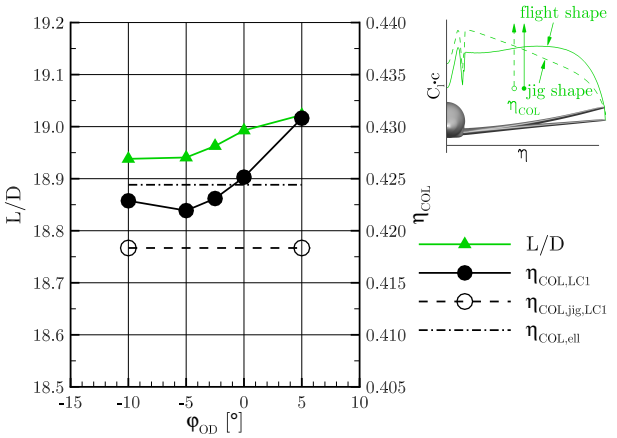

Fig. 8: Lift-to-drag ratio and center of lift under cruise flight conditions for global orthotropy angle variation with ply share optimization.

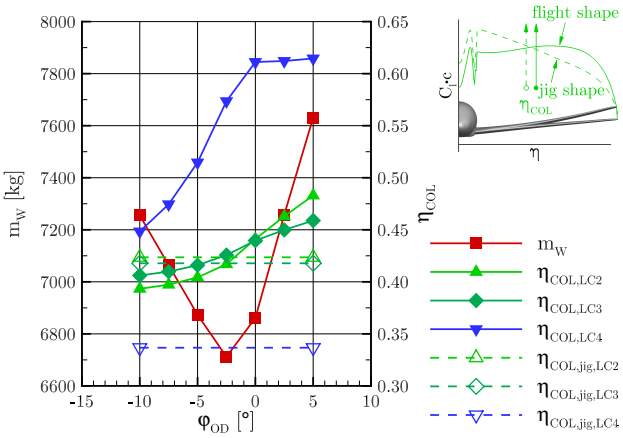

Fig. 9: Wing mass and center of lift under maneuver flight conditions for global orthotropy angle variation with fixed ply share.

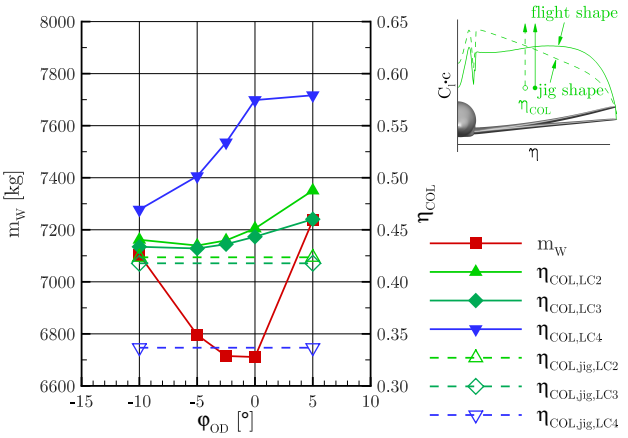

Fig. 10: Wing mass and center of lift under maneuver flight conditions for global orthotropy angle variation with ply share optimization.

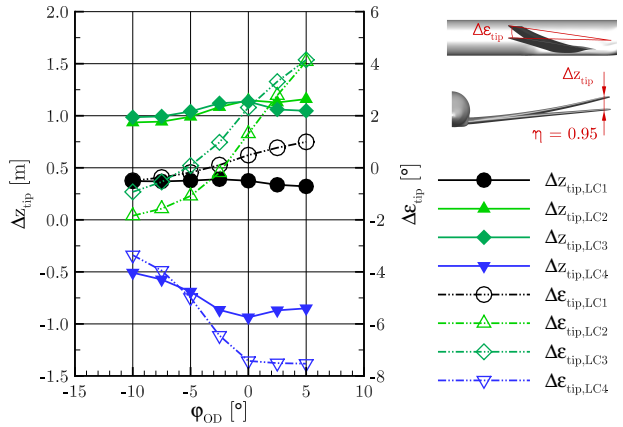

Fig. 11: Wing tip deformations for global orthotropy angle variation with fixed ply share.

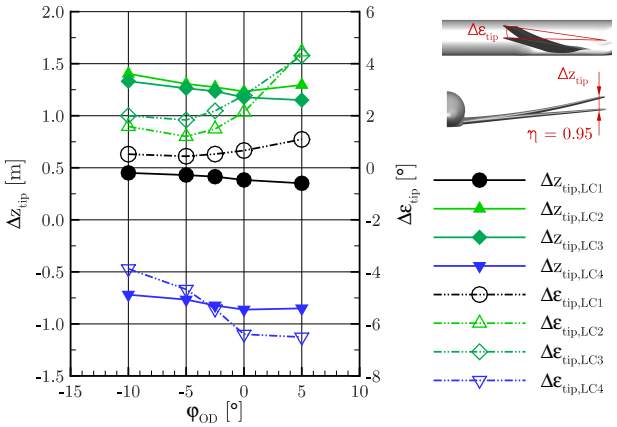

Fig. 12: Wing tip deformations for global orthotropy angle variation with ply share optimization.

board shift of the lift distribution. This means that with decreasing the global orthotropy angle an reversed bending-torsion coupling similar to backward swept wings can be achieved. For a value of $\varphi_{OD} \approx -2.5\,^\circ$ the shift of the center of lift is eliminated for the investigated cruise flight condition. A low level of bending-torsion coupling is beneficial for an natural laminar flow wing design, because the laminar-turbulent transition is sensitive to lift distribution changes.

The lift-to-drag ratio L/D correlates with the center of lift η_{COL} as expected. Thereby, the lift distribution in spanwise direction influences the induced drag and the transonic wave drag. The investigated forward swept wing shows the highest lift-to-drag ratio for an global orthotropy angle of $\varphi_{OD} = 5\,^\circ$ due to an improved lift distribution with low wave drag.

In Fig. 8 the lift-to-drag ratio L/D and the center of lift η_{COL} show a lower dependence on global orthotropy angle variation in comparison to the results with fixed ply share. The reason for this is that the ply share optimization reduces the number of 0-degree-layers dependent on the global orthotropy angle. Within the ply share optimization the wing mass is minimized under the constraint to fulfill all structural sizing criteria. This reduction of 0-degree-layers decreases the influence of the global orthotropy angle to the bending-torsion coupling.

In Fig. 9 and Fig. 10 the wing mass and the center of lift under maneuver flight conditions are shown for global orthotropy angle variation. Fig. 9 presents the results with fixed ply share and Fig. 10 shows the results with ply share optimization. In both figures the spanwise position of the center of lift for the "jig-shape" (index *jig*) is additionally included for each maneuver load case.

The influence of global orthotropy angle φ_{OD} to the wing mass m_W has been discussed before and is shown here again. In both 2.5g-maneuver load cases (LC2 and LC3) the center of lift η_{COL} shows the same trend for the global orthotropy angle φ_{OD} variation as under cruise flight conditions. As expected, an increased shift of the corresponding center of lift η_{COL} can be observed for both 2.5g-maneuver flights in comparison to the cruise flight. This means that with increasing global orthotropy angle φ_{OD} the center of lift η_{COL} is shifted further outboard as shown in Fig. 9. With global orthotropy angles of $\varphi_{OD} \leq -1\,^\circ$ an inboard shift of the center of lift can be achieved in comparison to the corresponding "jig-shape" for the maneuver load case LC2. For the maneuver load case LC3 global orthotropy angles of $\varphi_{OD} \leq -5\,^\circ$ are required to get an inboard shift of the center of lift. The center of lift for the -1g-maneuver load case (LC4) shows relative high values. This can be explained with high torsional moments in the outboard wing region due to pressure distributions with a significant leading edge suction peak. With increasing the global orthotropy angle φ_{OD} the center of lift η_{COL} is shifted outboard up to a value of $\eta_{COL} \approx 0.62$. The limit for the outboard shift of the center of lift can be explained with shock induced flow separations in the outboard wing region.

In Fig. 10 the wing mass m_W and the center of lift η_{COL} show a lower dependence on global orthotropy angle variation in comparison to the results with fixed ply share. Furthermore, no inboard shift of the center of lift is achieved for global orthotropy angle variation with ply share optimization. But the resulting wing masses of the global orthotropy angle variation with ply share optimization are lower than the values for the global orthotropy angle variation with fixed ply share.

In Fig. 11 and Fig. 12 the wing tip deformations under cruise flight (load case LC1) and maneuver flight conditions (load cases LC2, LC3 and LC4) are shown for global orthotropy angle variation. The wing tip deformations are evaluated at 95 % wingspan. Fig. 11 presents the results with fixed ply share and Fig. 12 shows the results with ply share optimization.

The bending deformations at the wing tip Δz_{tip} show low dependence on global orthotropy angle variation. The global orthotropy angle variation influences mainly the twist deformation at the wing tip. With increasing the global orthotropy angle φ_{OD} the twist angle at the wing tip $\Delta\varepsilon_{tip}$ increases continuously for the results in Fig. 11 with fixed ply share. For these results a global orthotropy angle φ_{OD} with zero twist deformation exist for each of the cruise flight and 2.5g-maneuver flight conditions. This means that a decoupling of bend and twist deformations can be achieved for a single load case. The results of Fig. 12 with ply share optimization show a lower dependence on the twist deformation with respect to global orthotropy angle variation.

4.3 Orthotropy angle variation in span direction

In this section the results of aeroelastic tailoring with different orthotropy angles in span direction are presented. The investigations has been performed with the different values for the inboard, middle wing and outboard orthotropy angles.

In Fig. 13 and Fig. 14 the results of wing mass for orthotropy angle variation in span direction are shown. Fig. 13 presents the results with fixed ply share and Fig. 14 shows the results with ply share optimization.

The orthotropy angle in the inboard wing region (different *line type*) shows the minimum of wing mass m_W for values of $\varphi_{OD,inboard} \approx 0\,^\circ$ as expected. This can explained with the limitation to control the bending-torsion coupling by aeroelastic tailoring due to the relatively small deformations in the inboard wing region compared to the middle and outboard wing. The variation of the middle wing orthotropy angle $\varphi_{OD,middle}$ (*x-axis*) shows the minimum of wing mass m_W for values between $\varphi_{OD,middle} = -5\,^\circ$ and $\varphi_{OD,middle} = 0\,^\circ$. With increasing the orthotropy angle in the outboard wing region $\varphi_{OD,outboard}$ (different *diagram*) an increasing wing mass m_W can be observed for the results with fixed ply share as shown in Fig. 13. The results with ply share optimization in Fig. 14 show a lower dependence on wing mass with respect to orthotropy angle variations in the outboard wing region.

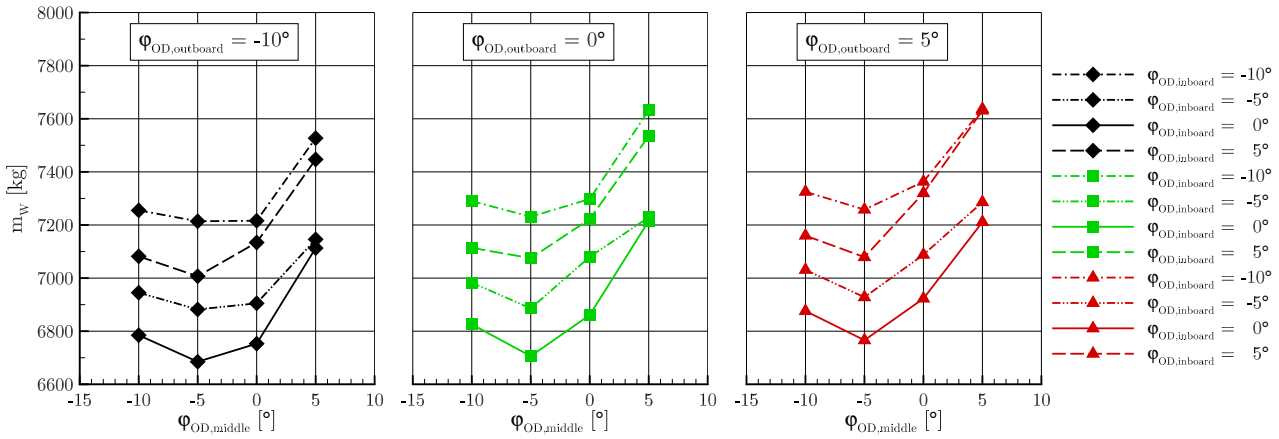

Fig. 13: Wing mass for orthotropy angle variation in span direction with fixed ply share.

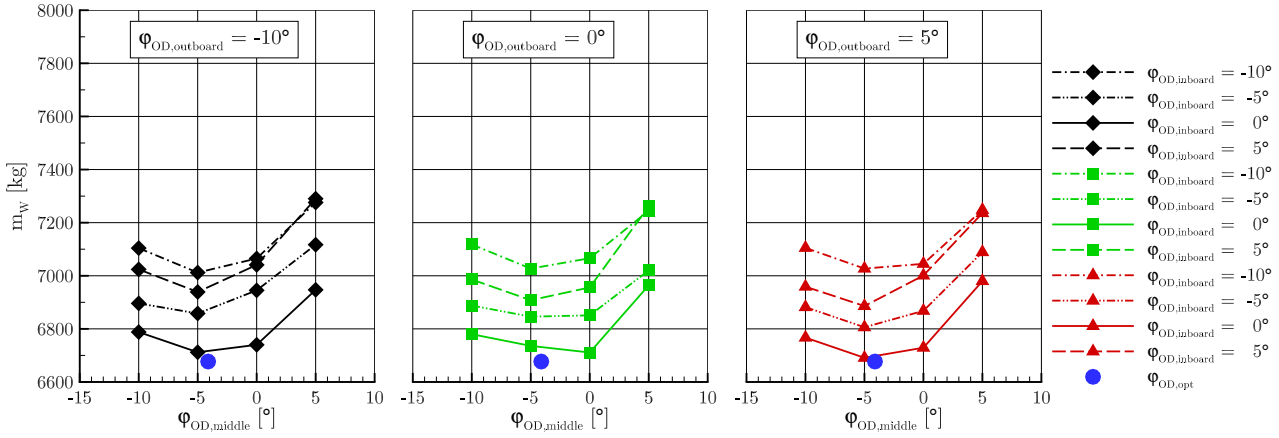

Fig. 14: Wing mass for orthotropy angle variation in span direction with ply share optimization.

In the next section the results for an orthotropy angle optimization are presented. The optimization has been performed with integrated ply share optimization in the structural sizing process. In Fig. 14 the optimal design in terms of minimal design mission fuel consumption is included (*blue point* with $\varphi_{OD,opt} = (0\,°; -4\,°; 1\,°)$).

4.4 Orthotropy angle optimization

The orthotropy angle optimization has been performed successfully for the selected design parameters and constraints. A surrogate based optimization (SBO) method has been selected for the orthotropy angle optimization. This optimization method searches the global optimum and offers a high level of robustness.

In Tab. 9 the orthotropy angles resulting from the optimization are shown for the baseline and the optimized wing. The orthotropy angle in the inboard wing region $\varphi_{OD,inboard}$ has been decreased to a value near zero in accordance with the results presented in Sec. 4.3. The orthotropy angle in the middle wing region has been increased to a value of $\varphi_{OD,middle} = -4\,°$. This negative value decreases the bending-torsion coupling to reduce the aerodynamic loads under maneuver flight conditions. Furthermore, the orthotropy angle in the outboard wing region $\varphi_{OD,outboard}$ is greater than the value of the baseline wing.

		Baseline	Optimized
Inboard orthotropy angle	$\varphi_{OD,inboard}$	$-10.0\,°$	$0.2\,°$
Middle wing orthotropy angle	$\varphi_{OD,middle}$	$-10.0\,°$	$-4.1\,°$
Outboard orthotropy angle	$\varphi_{OD,outboard}$	$-10.0\,°$	$1.0\,°$
Center of lift	$\eta_{COL,jig,LC1}$	0.4183	0.4183
	$\eta_{COL,LC1}$	0.4117	0.4240
	$\eta_{COL,LC2}$	0.3933	0.4438
	$\eta_{COL,LC3}$	0.4061	0.4387
	$\eta_{COL,LC4}$	0.4483	0.5450
Lift-to-drag ratio	L/D	18.81	18.97
Wing mass ratio	m_W/m_{MTO}	0.0989	0.0910
Fuel mass ratio	m_F/m_{MTO}	0.2134	0.2123
Payload ratio	m_P/m_{MTO}	0.2273	0.2363
Fuel consumption	FC	$1.57 \cdot 10^{-4}$/km	$1.50 \cdot 10^{-4}$/km

Table 9: Results of orthotropy angle optimization for baseline and optimized wing.

The results for the dimensionless span coordinate of the center of lift η_{COL} are additionally included in Tab. 9. These values correspond with the lift distributions given in Fig. 15, Fig. 16, Fig. 17 and Fig. 18. For the cruise flight condition the position of the center of lift is also given for the "jig-shape" wing geometry. The load shift in spanwise direction between the "jig-shape" and the "flight-shape" indicates the lift distribution changes with respect to wing deformations due to static aeroelastic effects. Consequently, the center of lift variation with respect to wing deformations under cruise flight conditions are relatively small and in the same order for both wings. This is beneficial for an natural laminar flow wing design, because the laminar-turbulent transition is sensitive to lift distribution changes.

The optimization results for the lift-to-drag ratio, the wing mass ratio, the fuel mass ratio, the payload ratio and the design mission fuel consumption are also given in Tab. 9. These results show an increased aerodynamic performance in terms of lift-to-drag ratio L/D and simultaneously an decreased wing mass m_W/m_{MTO} for the optimized wing in comparison to the baseline wing. The increased lift-to-drag-ratio can be explained with the induced drag reduction resulting from a more elliptical lift distribution and inboard wave drag reduction due to a lower inboard lift coefficient. This leads to the reduced fuel mass ratio. Consequently the payload ratio m_P/m_{MTO} increases. The main result of the orthotropy angle optimization is the reduction of the fuel consumption FC in the order of 4 %.

In Fig. 15, an overview of the orthotropy angle optimization results for cruise flight condition is given. This includes the comparison of the baseline and the optimized wing in terms of isentropic Mach number distribution for the upper wing, the deformations for the 1g-cruise flight and the corresponding lift and lift coefficient distributions in span direction. For each lift distribution the related elliptical lift distribution is shown by a dot-dashed line as a reference. The elliptical lift distribution is the optimum for planar wings in terms of induced drag. The optimized wing shows an outboard load shift and bending deformations with similar amplitude in comparison to the baseline wing.

Fig. 16 and Fig. 17 show the results for the 2.5g-maneuver load cases LC 2 and LC 3 in a similar form. An increased bending deformation of the optimized wing is observed for both maneuver flight conditions. Thereby, an inboard load shift is observed for the baseline wing under both maneuver flight conditions in comparison to the cruise flight. In contrast, the results for the optimized wing show an outboard load shift for both maneuver flight conditions. These load shifts in opposite direction can be explained with the reduced orthotropy angles of the optimized wing to control the geometrical bending-torsion coupling of the forward swept wing.

In Fig. 18, an overview of the orthotropy angle optimization results for the -1.0g-maneuver load case LC 4 is given. This includes the comparison of the baseline and the optimized wing in terms of isentropic Mach number distribution for the lower wing, the deformations and the corresponding lift and lift coefficient distributions in span direction. An increased bending deformation of the optimized wing is observed. Thereby, the optimized wing is more outboard loaded in comparison to the baseline wing. This is a result of the increased bending deformation and the more pronounced positive bending-torsion coupling due to reduced orthotropy angles.

The lift distributions of the investigated maneuver load cases show the importance of considering the static aer-

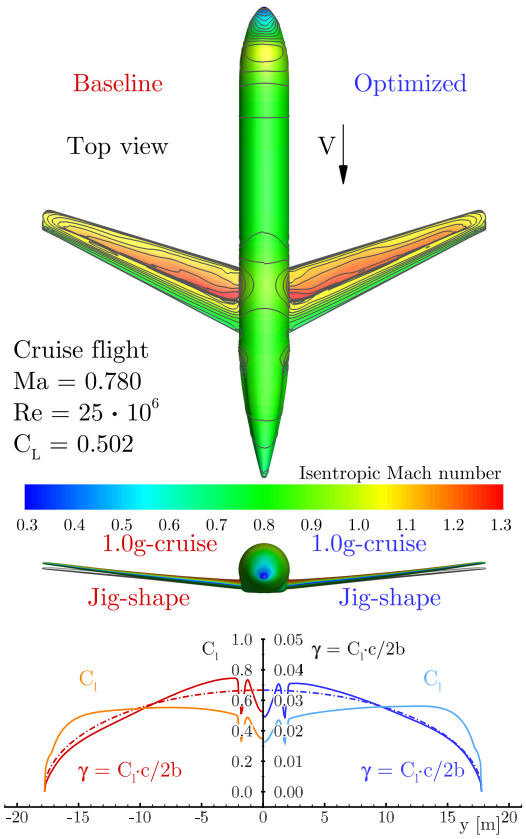

Fig. 15: Overview of optimization results for cruise flight.

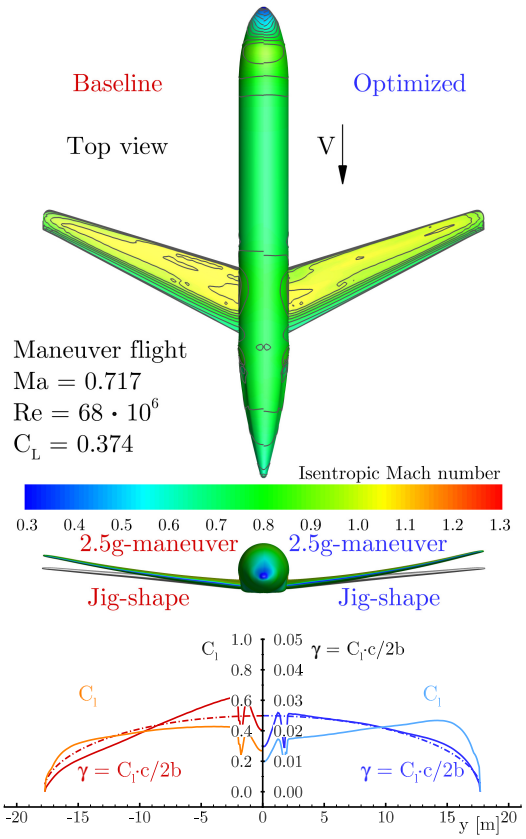

Fig. 16: Overview of optimization results for load case LC2.

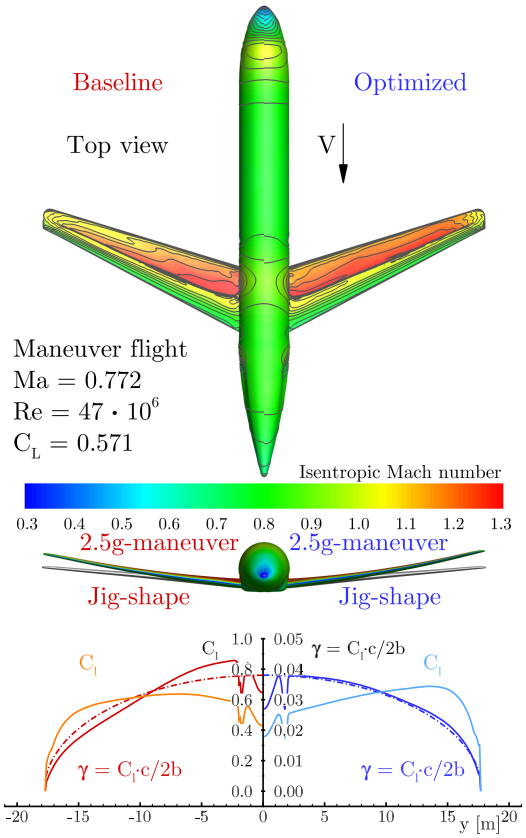

Fig. 17: Overview of optimization results for load case LC3.

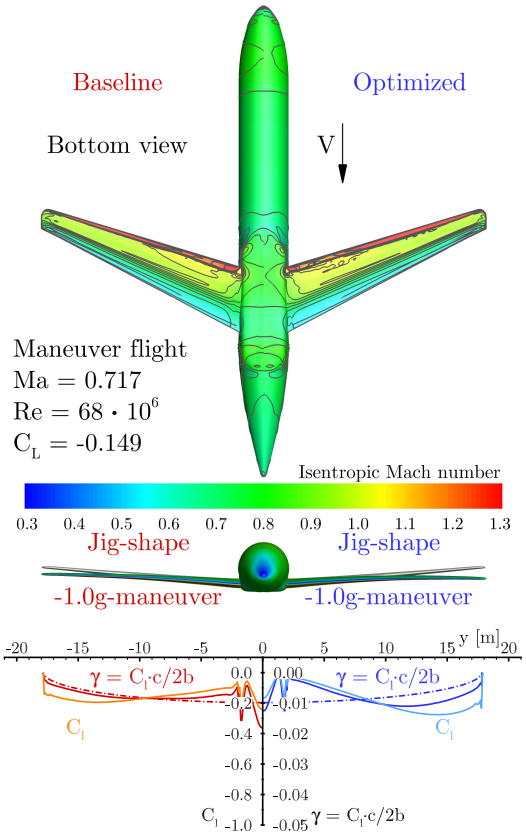

Fig. 18: Overview of optimization results for load case LC4.

oelastic effects in the loads computation for the structural wing sizing. Furthermore, the results show that an adequate level of aeroelastic tailoring at the correct position lead to reduced wing mass and minimum design mission fuel consumption.

5 CONCLUSION AND OUTLOOK

In the national joint research project AeroStruct an integrated process chain for aerostructural wing analysis based on high fidelity simulation methods has been developed. This process chain has been applied to investigate the aeroelastic tailoring for an NLF forward swept wing. The aeroelastic tailoring has been used to counteract the susceptibility of forward swept wings to static divergence. Thereby, variations of the orthotropy angle of the composite material has been studied to control the bending-torsion coupling and to get a positive influence on the static aeroelastic effects.

The application of aeroelastic tailoring for structural mass reduction is a trade-off between aerodynamic load reduction and fiber orientation in internal load direction. In the structural wing sizing process the options of fixed ply share and of integrated ply share optimization have been investigated. The results show that the sizing with fixed ply share allows a better control of the bending-torsion coupling but leads to higher wing masses compared to the sizing with ply share optimization.

For the assessment of the wing design the influence to cruise flight performance have to be considered as well. The usage of the integrated process chain combines the aerodynamic performance prediction and the wing mass estimation based on structural wing sizing for essential load cases. Thereby, the static aeroelastic effect are considered for the cruise flight and all selected maneuver load cases. The minimization of design mission fuel has been used as objective function for the wing design studies and optimization.

The results of the design studies show that the global orthotropy angle allows the control of the bending-torsion coupling. To get wing designs with low wing masses and minimum design mission fuel consumption the aeroelastic tailoring in the inboard wing region should not be used to control the bending-torsion coupling. An aeroelastic tailoring in the middle wing region is the most efficient way to reduce the outboard load shift for the NLF forward swept wing design considered here. The orthotropy angle optimization shows an reduced aeroelastic tailoring and a more outboard position of the center of lift for the design maneuver load cases in comparison to the baseline design. However, the optimization results show a wing mass reduction in the order of 8 % and design mission fuel consumption reduction in the order of 4 %.

Furthermore, the center of lift variation with respect to wing deformations under cruise flight conditions are relatively small for both wings and the suitability for a robust NLF wing design has to be proven. But the design studies include a wing design with a wing mass penalty in the order of 50 kg and practically eliminated bending-torsion coupling under cruise flight conditions.

The next step is the development and integration of a more advanced structural sizing and optimization process for composite materials. This new process allows the usage of the ply share as global design parameter to consider the aeroelastic effects in the ply share optimization. Furthermore, the structural design and material properties have to be adopted to investigate the aeroelastic tailoring on more flexible wing designs.

The cruise flight performance of NLF wing designs is highly sensitive to the extension of laminar flow. To improve the aerodynamic performance prediction, the integration of a laminar-turbulent transition prediction method into the aerostructural process chain is planned. This extension of the process chain allows a more realistic consideration of the interactions between wing deformations and cruise flight performance for NLF wing designs.

Acknowledgements The LuFo IV joint research project AeroStruct upon which this publication is based has been funded by the German Federal Ministry for Economic Affairs and Energy (BMWi) under the project number 20A1102A.

The authors wish to thank the Institute of Aerodynamics and Flow Technology and the Institute of Composite Structures and Adaptive Systems for providing the support of many colleagues, the IT infrastructure and the computing resources for the complex computations.

References

[1] European Commision. *European Aeronautics: A Vision for 2020*. Luxembourg, Belgium: Office for Official Publications of the European Communities, 2001.

[2] European Commision. *2008 Addendum to the Strategic Research Agenda*. http://www.acare4europe.com. 2008.

[3] European Commision. *Flightpath 2050 Europe's Vision for Aviation*. Luxembourg, Belgium: Office for Official Publications of the European Communities, 2011.

[4] N. Kroll et al. 'The MEGAFLOW-Project - Numerical Flow Simulation for Aircraft'. In: *Progress in Industrial Mathematics at ECMI 2004* (2005), pp. 3–33.

[5] N. Kroll et al. 'Ongoing Activities in Shape Optimization Within The German Project MEGADESIGN'. In: *ECCOMAS 2004*. 2004.

[6] N. Kroll et al. 'Flow Simulation and Shape Optimization For Aircraft Design'. In: *Journal of Computational and Applied Mathematics* 203 (Dec. 2005), pp. 397–411.

[7] N. Kroll et al. 'Ongoing Activities in Flow Simulation and Shape Optimization within the German Megadesign Project'. In: *ICAS 2006, 25th International Congress of the Aeronautical Sciences*. 2006.

[8] N. Kroll et al. *MEGADESIGN and MegaOpt - German Initiatives for Aerodynamic Simulation and Optimization in Aircraft Design*. Springer-Verlag Berlin Heidelberg, 2009.

[9] N. R. Gauger. 'Ongoing activities in shape optimization within the German project MEGADESIGN'. In: *EUCCO2004, Dresden (de), 29.-31.03.2004*. 2004.

[10] M. H. Shirk et al. 'Aeroelastic tailoring - Theory, practice, and promise'. In: *Journal of Aircraft* 23.1 (1986), pp. 6–18.

[11] C. V. Jutte and B. K. Stanford. *Aeroelastic Tailoring of Transport Aircraft Wings State-of-the-Art and Potential Enabling Technologies*. Tech. rep. NASA/TM-2014-218252. National Aeronautics and Space Administration, 2014.

[12] S. Dähne et al. 'Steps to Feasibility for Laminar Wing Design in a Multidisciplinary Environment'. In: *ICAS 2014*. Sept. 2014.

[13] K. Horstmann and T. Streit. 'Aerodynamic Wing Design for Transport Aircraft - Today: Hermann Schlichting - 100 Years'. In: ed. by R. Radespiel et al. Vol. 102. Springer-Verlag Berlin Heidelberg, 2009, pp. 130–144.

[14] G. Schrauf. 'Status and perspectives of laminar flow'. In: *The Aeronautical Journal* 109.1102 (Dec. 2005), pp. 639–644.

[15] J. E. Green. 'Laminar Flow Control - Back to the Future?' In: *38th Fluid Dynamics Conference and Exhibit, Seattle, Washington, USA*. AIAA 2008-3728. 2008.

[16] A. Seitz et al. 'The DLR Project LamAiR: Design of a NLF Forward Swept Wing for Short and Medium Range Transport Application'. In: *29th AIAA Applied Aerodynamics Conference*. AIAA Conference Paper AIAA 2011-3526. June 2011.

[17] G. Redeker and G. Wichmann. 'Forward Sweep - A Favourable Concept for a Laminar Flow Wing'. In: *Journal of Aircraft* 28 (1991), pp. 97–103.

[18] M. Kruse et al. 'A Conceptual Study of a Transonic NLF Transport Aircraft with Forward Swept Wings'. In: *30th AIAA Applied Aerodynamics Conference, New Orleans, Louisiana*. AIAA Conference Paper AIAA 2012-3208. June 2012.

[19] T. F. Wunderlich. 'Multidisciplinary wing optimization of commercial aircraft with consideration of static aeroelasticity'. In: *CEAS Aeronautical Journal* 6.3 (2015), pp. 407–427.

[20] T. F. Wunderlich et al. 'Multidisciplinary Optimization of a NLF Forward Swept Wing in combination with Aeroelastic Tailoring using CFRP'. In: *Deutscher Luft- und Raumfahrtkongress 2015*. Nov. 2015.

[21] A. B. Lambe and J. R. R. A. Martins. 'Extensions to the Design Structure Matrix for the Description of Multidisciplinary Design Analysis and Optimization Processes'. In: *Structural and Multidisciplinary Optimization* 46 (2012), pp. 273–284.

[22] R. Kamakoti and W. Shyy. 'Fluid-structure interaction for aeroelastic applications'. In: *Progress in Aerospace Sciences* 40.8 (2005), pp. 535–558.

[23] X. B. Lam et al. 'Coupled Aerostructural Design Optimization Using the Kriging Model and Integrated Multiobjective Optimization Algorithm'. In: *Journal of Optimization Theory and Applications* 142.3 (2009), pp. 533–556.

[24] D. P. Raymer. *Aircraft Design: A Conceptual Approach*. Third Edition. American Institute of Aeronautics and Astronautics, 1999.

[25] C. M. Liersch and M. Hepperle. 'A Unified Approach for Multidisciplinary Preliminary Aircraft Design'. In: *CEAS European Air and Space Conference, Manchester, United Kingdom*. 2009.

[26] M. Galle. *Ein Verfahren zur numerischen Simulation kompressibler, reibungsbehafteter Strömungen auf hybriden Netzen*. Tech. rep. DLR-Forschungsbericht 99-04. Braunschweig: DLR Institut für Aerodynamik und Strömungstechnik, 1999.

[27] T. Gerhold. 'Overview of the Hybrid RANS TAU-Code, In: Kroll N., Fassbender J. (Eds) MEGAFLOW - Numerical Flow Simulation Tool for Transport Aircraft Design'. In: *Notes on Multidisciplinary Design* 89 (2005).

[28] D. Schwamborn et al. 'The DLR TAU-Code: Recent Applications in Research and Industry'. In: *European Conference on Computational Fluid Dynamics, ECCOMAS CFD 2006 Conference, Delft, The Netherlands*. 2006.

[29] N. Kroll and J. K. Fassbender. 'MEGAFLOW - Numerical Flow Simulation for Aircraft Design, Braunschweig'. In: *Notes on Numerical Fluid Mechanics and Multidisciplinary Design (NNFM)* 89 (2002).

[30] N. Kroll et al. 'MEGAFLOW - A Numerical Flow Simulation Tool For Transport Aircraft Design, Toronto, Canada'. In: *ICAS Congress 2002*. 2002, pp. 1.105.1–1.105.20.

[31] S. R. Allmaras et al. 'Modifications and Clarifications for the Implementation of the Spalart-Allmaras Turbulence Model'. In: *Seventh International Conference on Computational Fluid Dynamics (ICCFD7)*. 2012, pp. 1–11.

[32] S. Freund et al. 'Parametric Model Generation and Sizing of Lightweight Structures for a Multidisciplinary Design Process'. In: *NAFEMS Konferenz: "Berechnung und Simulation - Anwendungen, Entwicklungen, Trends*. May 2014.

[33] M.-H.-1.-3. Military. *Composite Materials Handbook, Polymer Matrix Composites: Materials Usage, Design, and Analysis*. Vol. 3 of 5. US Department of Defense, June 2002.

[34] L. J. Hart-Smith. 'The Ten-Percent Rule for Preliminary Sizing of Fibrous Composite Structures'. In: *51st Annual Conference, Hartford, Connecticut*. Society of Allied Weight Engineers, Inc., May 1992, p. 28.

[35] H. Barnewitz and B. Stickan. 'Improved Mesh Deformation'. In: *Notes on Numerical Fluid Mechanics and Multidisciplinary Design*. Ed. by B. Eisfeld et al. Vol. 122. 2013, pp. 219–243.

[36] M. Kintscher et al. 'Design of a smart leading edge device for low speed wind tunnel tests in the European project SADE'. In: *International Journal of Structural Integrity* 2.4 (2011), pp. 383–405.

[37] G. K. W. Kenway et al. 'Aerostructural optimization of the Common Research Model configuration'. In: *15th AIAA/ISSMO Multidisciplinary Analysis and Optimization Conference, Georgia, USA*. June 2014.

[38] T. F. Wunderlich. 'Multidisziplinärer Entwurf und Optimierung von Flügeln für Verkehrsflugzeuge'. In: *Deutscher Luft- und Raumfahrtkongress, Aachen*. DGLR-Tagungsband - Ausgewählte Manuskripte DLRK2009-1181. Sept. 2009.